Available online at www.sciencedirect.com
ScienceDirect
Journal of Sound and Vibration 301 (2007) 803–820
JOURNAL OF SOUND AND VIBRATION
www.elsevier.com/locate/jsvi

Free and forced vibration analysis using the smoothed finite element method (SFEM)

K.Y. Dai[a,b,*], G.R. Liu[a,b]

[a]*Center for Advanced Computations in Engineering Science (ACES), Department of Mechanical Engineering, National University of Singapore, 10 Kent Ridge Crescent 119260, Singapore*
[b]*Singapore-MIT Alliance (SMA), E4-04-10, 4 Engineering Drive 3, Singapore 117576, Singapore*

Received 2 August 2006; received in revised form 21 September 2006; accepted 28 October 2006
Available online 18 December 2006

Abstract

Smoothed finite element method (SFEM) was recently proposed by the authors to improve the accuracy and convergence rate of the existing standard four-node isoparametric finite element method (FEM) by 2×2 quadrature in the static analysis. In this work, it is further extended to the free and forced analysis of two-dimensional (2D) dynamic problems. It is found that SFEM achieves more accurate results and higher convergence rates as compared with the corresponding finite elements in solving dynamic problems without increasing the computational cost. As only shape function itself is involved in computing the field gradients and no coordinate transformation is required, the method is very easy to implement. Nonlinear elastic forced vibration problem is also examined by using smoothed deformation gradients on each cell.

1. Introduction

Smoothed finite element method (SFEM) was recently presented by Liu et al. [1] by incorporation of the strain smoothing operation with the existing finite element techniques. The SFEM shows some superior features over the original FEM. Due to the introduced strain projection technique only shape function itself is involved in the calculation of field gradients and no coordinate transformation is necessary. Correspondingly, the shape of element in SFEM can be of arbitrary shape. Numerical results in their work have demonstrated that SFEM gives more accurate results in both primary variables and derivative ones and their convergence rates have also been improved to some extent. Most importantly, these good features are acquired without increasing the number of field nodes and computational cost as compared with the 4-node isoparametric finite elements. The numerical procedure is comparably even simpler and more straightforward.

Later on they proved that SFEM is an energy-consistent method [2] and its upper and lower bound solution can be obtained by adjusting the number of smoothing cells (SC) by which an element is subdivided for stable

*Corresponding author. Singapore-MIT Alliance (SMA), E4-04-10, 4 Engineering Drive 3, Singapore 117576, Singapore. Tel.: +65 6516 4796; fax: +65 6775 2920.
E-mail address: smadky@nus.edu.sg (K.Y. Dai).

0022-460X/$ - see front matter © 2006 Elsevier Ltd. All rights reserved.
doi:10.1016/j.jsv.2006.10.035

integration of energy. In particular if an entire element is used as one SC, an upper bound solution can be acquired that corresponds to that of the finite element equilibrium model. On the contrary, with the increase of the number of SC the solution approaches its lower bound solution, which can be obtained using the displacement-compatible finite element model. In the process of increasing the SC the SFEM solution will transform monotonically from the upper to the lower bound.

In this work, the SFEM is further extended to the free and forced vibration analysis of 2D problems. Four-node quadrilateral elements are used and each is subdivided into four SC in the calculation of stiffness matrix. Similar type of finite elements (isoparametric elements by 2×2 quadrature and quintessential bending/incompressible (QBI), elements) is also employed in the analysis and the accuracies of the two methods are compared. In the forced vibration analysis, both explicit and implicit time integration schemes are used. Geometrical nonlinearity is considered in the explicit nonlinear analysis. Total Lagrange formulation and central difference procedure are adopted. Deformation gradients are smoothed on the level of SC in the initial configuration. Several numerical examples are analyzed to demonstrate the accuracy, stability and effectiveness of the SFEM.

2. Discrete governing equations

Consider a deformable body occupying domain Ω in motion, subjected to body forces $\mathbf{b}$, external applied tractions $\mathbf{t}$ on boundary Γ_t and displacement boundary conditions $\mathbf{u} = \bar{\mathbf{u}}$ on Γ_u. It undergoes arbitrary virtual displacements $\delta\mathbf{d}$, which accordingly give rise to compatible virtual strains $\delta\boldsymbol{\varepsilon}$ and internal displacements $\delta\mathbf{u}$. If the inertial and damping forces are also considered in the dynamic equilibrium equations, the principle of virtual work requires that

$$\int_\Omega \delta\boldsymbol{\varepsilon}^{\mathrm{T}}\boldsymbol{\sigma}\,\mathrm{d}\Omega - \int_\Omega \delta\mathbf{u}^{\mathrm{T}}[\mathbf{b} - \rho\ddot{\mathbf{u}} - c\dot{\mathbf{u}}]\,\mathrm{d}\Omega - \int_{\Gamma_t} \delta\mathbf{u}^{\mathrm{T}}\mathbf{t}\,\mathrm{d}\Gamma = 0. \tag{1}$$

By means of the spatial discretization procedure in the FEM, the virtual displacements and strains within any element can be written as

$$\delta\mathbf{u}^h = \sum_I \mathbf{N}_I \delta\mathbf{d}_I, \quad \mathbf{u}^h = \sum_I \mathbf{N}_I \mathbf{d}_I, \tag{2}$$

$$\delta\boldsymbol{\varepsilon}^h = \sum_I \mathbf{B}_I \delta\mathbf{d}_I, \quad \boldsymbol{\varepsilon}^h = \sum_I \mathbf{B}_I \mathbf{d}_I, \tag{3}$$

where $\mathbf{d}_I = [u_I \quad v_I]^{\mathrm{T}}$ is the nodal displacement vector, and $\mathbf{B}$ is the standard displacement gradient matrix. In 2D linear elastic problems it is given as

$$\mathbf{B}_I = \nabla_S N_I(x) = \begin{bmatrix} N_{I'x} & 0 \\ 0 & N_{I'y} \\ N_{I'y} & N_{I'x} \end{bmatrix}. \tag{4}$$

And the stress is obtained by generalized Hooke's law as $\boldsymbol{\sigma}^h = \mathbf{D}\,\boldsymbol{\varepsilon}^h$.

The energy assembly process gives

$$\int_\Omega \delta\mathbf{d}^{\mathrm{T}}\mathbf{B}^{\mathrm{T}}\boldsymbol{\sigma}\,\mathrm{d}\Omega - \int_\Omega \delta\mathbf{d}^{\mathrm{T}}\mathbf{N}^{\mathrm{T}}[\mathbf{b} - \rho\ddot{\mathbf{u}} - c\dot{\mathbf{u}}]\,\mathrm{d}\Omega - \int_{\Gamma_t} \delta\mathbf{d}^{\mathrm{T}}\mathbf{N}^{\mathrm{T}}\mathbf{t}\,\mathrm{d}\Gamma = 0. \tag{5}$$

Since the expressions hold for any arbitrary virtual displacements $\delta\mathbf{d}$, one gets

$$\int_\Omega \mathbf{B}^{\mathrm{T}}\boldsymbol{\sigma}\,\mathrm{d}\Omega - \int_\Omega \mathbf{N}^{\mathrm{T}}[\mathbf{b} - \rho\ddot{\mathbf{u}} - c\dot{\mathbf{u}}]\,\mathrm{d}\Omega - \int_{\Gamma_t} \mathbf{N}^{\mathrm{T}}\mathbf{t}\,\mathrm{d}\Gamma = 0. \tag{6}$$

Then the discrete governing equation can be written as

$$\mathbf{f}^{\mathrm{int}} - \mathbf{f}^{\mathrm{ext}} + \mathbf{f}^I + \mathbf{f}^D = \mathbf{0} \tag{7}$$

or

$$\mathbf{M}\ddot{\mathbf{d}} + \mathbf{C}\dot{\mathbf{d}} + \mathbf{f}^{\text{int}} = \mathbf{f}^{\text{ext}}, \tag{8}$$

where $\mathbf{d}$ is the vector of general nodal displacements and

$$\mathbf{f}^{\text{int}} = \int_{\Omega} \mathbf{B}^{\mathrm{T}}\boldsymbol{\sigma}\,\mathrm{d}\Omega, \tag{9}$$

$$\mathbf{f}^{\text{ext}} = \int_{\Omega} \mathbf{N}^{\mathrm{T}}\mathbf{b}\,\mathrm{d}\Omega + \int_{\Gamma_t} \mathbf{N}^{\mathrm{T}}\mathbf{t}\,\mathrm{d}\Gamma, \tag{10}$$

$$\mathbf{M} = \int_{\Omega} \mathbf{N}^{\mathrm{T}}\boldsymbol{\rho}\mathbf{N}\,\mathrm{d}\Omega, \tag{11}$$

$$\mathbf{C} = \int_{\Omega} \mathbf{N}^{\mathrm{T}}\mathbf{c}\mathbf{N}\,\mathrm{d}\Omega. \tag{12}$$

In SFEM, the smoothed strain is obtained using the following strain smoothing operation, which is very similar to the mean dilatation procedure used to deal with the incompressibility in nonlinear mechanics [3,4]

$$\tilde{\boldsymbol{\varepsilon}}^h = \int_{\Omega_C} \boldsymbol{\varepsilon}^h(\mathbf{x})\Phi(\mathbf{x})\,\mathrm{d}\Omega, \tag{13}$$

where $\boldsymbol{\varepsilon}^h = \nabla_S \mathbf{u}^h$ is the strain obtained from the displacement compatibility condition as given in Eq. (3). Ω_C is the domain of a smoothing cell on which the smoothing operation is performed. The smoothed operation was recently used in weak-form meshless method based on nodal integration [5,6]. Depending on the stability analysis [1], Ω_C may be an entire element or part of an element as shown in Fig. 1. Φ is a smoothing function and defined as

$$\Phi(\mathbf{x} - \mathbf{x}_C) = \begin{cases} 1/A_C & \mathbf{x} \in \Omega_C, \\ 0 & \mathbf{x} \notin \Omega_C, \end{cases} \tag{14}$$

where $A_C = \int_{\Omega_C} \mathrm{d}\Omega$, the area of smoothing cell. The element area is the summation of its SC, $A_e = \sum_C^{\text{SC}} A_C$ with SC being the number of the cells that an element is subdivided.

Substituting Φ and $\mathbf{u}^h$ into Eq. (13) one can get the smoothed gradients of displacement

$$\tilde{\boldsymbol{\varepsilon}}^h(\mathbf{x}_C) = \int_{\Gamma_C} \mathbf{n}(\mathbf{x})\mathbf{u}^h(\mathbf{x})\Phi(\mathbf{x} - \mathbf{x}_C)\,\mathrm{d}\Gamma = \frac{1}{A_C}\int_{\Gamma_C} \mathbf{n}(\mathbf{x})\mathbf{u}^h(\mathbf{x})\,\mathrm{d}\Gamma, \tag{15}$$

where Γ_C is the boundary of the smoothing cell and n is the matrix of outward unit normal. Note that the choice of constant Φ degenerates the volume integration into contour integration around the boundaries of the

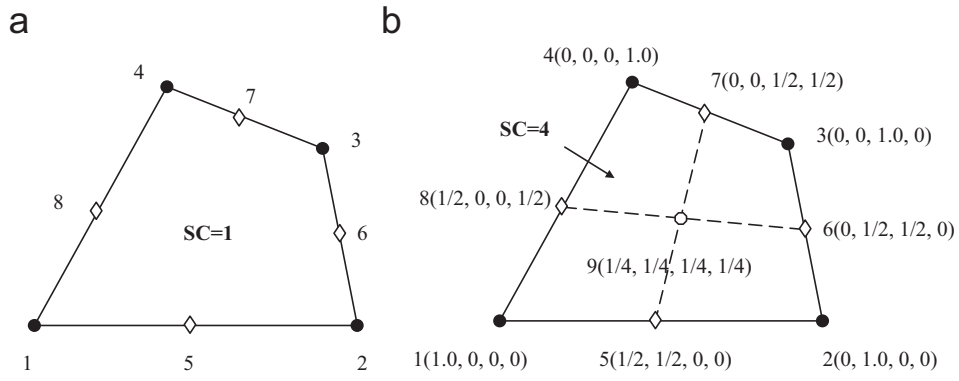

Fig. 1. Subdivision of smoothing cells and the values of shape functions.

smoothing cell in Eq. (13). Particularly in 2D linear elasticity problems the smoothed strain in discrete form can be described as

$$\tilde{\boldsymbol{\varepsilon}}^h(\mathbf{x}_C) = \sum_I^n \tilde{\mathbf{B}}_I(\mathbf{x}_C)\mathbf{d}_I, \tag{16}$$

where n is the number of element nodes. $\tilde{\mathbf{B}}_I$ is the smoothed strain matrix as

$$\tilde{\mathbf{B}}_I(\mathbf{x}_C) = \begin{bmatrix} \tilde{b}_{I1}(\mathbf{x}_C) & 0 \\ 0 & \tilde{b}_{I2}(\mathbf{x}_C) \\ \tilde{b}_{I2}(\mathbf{x}_C) & \tilde{b}_{I1}(\mathbf{x}_C) \end{bmatrix}. \tag{17}$$

If one Gaussian point is used for line integration along each segment of the edge ${\Gamma_i}^C$ of Ω_C, Eq. (17) can be transformed to its algebraic form

$$\tilde{b}_{Ik}(\mathbf{x}_C) = \sum_{i=1}^{M} \frac{1}{A_{Ci}} N_I(\mathbf{x}_i^{\mathrm{GP}}) n_{ik}^C l_i^C \quad (k = 1, 2), \tag{18}$$

where ${\mathbf{x}_i}^{\mathrm{GP}}$ is the midpoint (Gaussian point) of boundary segment of ${\Gamma_i}^C$, whose length and outward unit normal are denoted as ${l_i}^C$ and ${n_i}^C$, respectively.

Now the internal nodal force in SFEM is expressed as

$$\mathbf{f}_C^{\mathrm{int}} = \int_{\Omega_C} \tilde{\mathbf{B}}^{\mathrm{T}} \tilde{\boldsymbol{\sigma}} \, \mathrm{d}\Omega. \tag{19}$$

The smoothed stress $\tilde{\boldsymbol{\sigma}}$ is obtained in the same way from the $\tilde{\boldsymbol{\varepsilon}}^h$ as in FEM, which is constant over a smoothing cell. In particular, for linear elastic problems, $\tilde{\boldsymbol{\sigma}} = \mathbf{D}\tilde{\boldsymbol{\varepsilon}}^h$ is calculated on the level of smoothing cell. The summation of those corresponding to each of the SC in an element leads to the element internal force vector.

3. Numerical implementation

3.1. Stability condition

In this work four-node quadrilateral element is employed for domain discretization. In the single-element eigenvalue analysis we performed, it is found that spurious zero-energy mode appears and one smoothing cell (SC = 1) is equivalent to three independent strain relations ($n_\sigma = 3$). If the element is fixed by three constraints (rigid-body movements) the problem is still singular as $n_\sigma < n_u = 4 \times 2 - 3 = 5$, where n_u is the number of the displacement freedoms. It is easy to verify that the stiffness matrix obtained using one SC in SFEM is identical to that of 4-node finite element with one-point quadrature. Therefore, the same eigenvalues are obtained using FEM (Q1) and SFEM (SC = 1) as long as they employ the same mass matrix. If the element is subdivided into four quadrilateral SC (SC = 4) using four midpoints on each side of an element, as shown in Fig. 1(b), we have $n_\sigma = 4 \times 3 = 12 > n_u$ and now the integration is stable and thus solvable. Further increase of SC also yields a stable integration but the computational cost is also increased accordingly and the accuracy may not be better, as shown in the following examples. Therefore if not specified otherwise, we always use four quadrilateral cells (SC = 4) for a four-node element in this work. Generally, to ensure stability condition, a necessary requirement should be satisfied, i.e., $n_\sigma > n_u$. The issue on how to determine a suitable number of SC for more general cases such as a polygonal element, has been detailed by Dai et al. [7].

3.2. Shape function construction and standard patch test

In the SFEM only shape functions are needed to calculate the smoothed strains at some discrete points of an element and no shape function derivatives are involved. Hence it is very convenient to construction SFEM shape functions. Many approaches are suggested in literature [1]. In this work, a very simple way is

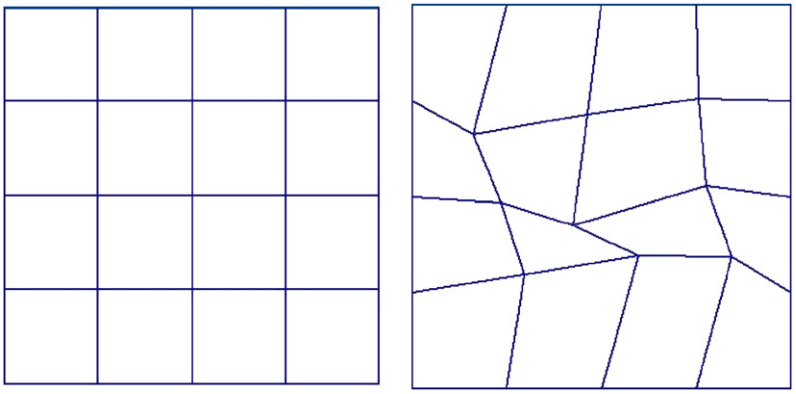

Fig. 2. The 4×4 element meshes for standard patch test.

recommended as shown in Fig. 1(b). The shape function values at the midpoint on a side of element are calculated on the average using two related nodes and midpoints on the cell edges can be obtained in a similar way. It is noticed that shape functions constructed in this way maintain the good properties in FEM, such as Delta function property, partition of unity, linear consistency, linear geometric compatibility and positivity within an element. Note that due to the Delta property of its shape functions, boundary conditions can be implemented in the same way as in FEM.

To verify these properties, a standard patch test is carried out for a patch made up of 4×4 element meshes as shown in Fig. 2. All the boundary nodes of the patch are constrained using constant/linear displacement patterns in two directions. It is found that all the inner nodes follow exactly (to machine precision) the same constant/linear displacement patterns we imposed on boundary nodes. This phenomenon can be easily explained from the specially devised shape functions that have linear geometric compatibility. Furthermore, the points on edges of each cell also maintain this property. Unfortunately, due to the adoption of the smoothed operation of displacement gradients, the interior points inside any cell will violate this condition, which makes the method variationally incompatible. Instead the operation makes these points inside a cell have a constant strains and stresses and thus satisfy the equilibrium equations. So the smoothing operation is also called "an equilibrator" by Liu et al. [2].

3.3. Mass matrix

In the four-node elements of SFEM, as each of them is subdivided into four cells for integration and their areas are also involved in the determination of displacement gradients, it is very natural and convenient to use lumped mass matrix in dynamic analysis, which is given as

$$\mathbf{M}_e = \mathrm{diag}\{m_1 \quad m_1 \quad m_2 \quad m_2 \quad m_3 \quad m_3 \quad m_4 \quad m_4\}, \tag{20}$$

where $m_i = \rho t A_{Ci}$ $(i = 1, \ldots, 4)$ is the mass of ith cell corresponding to local node i, and ρ and t are the mass density and the thickness of the cell, respectively. The diagonal form of lumped mass matrix shows superiority over the consistent mass matrix in data recording and algebraic equation solving, especially in the explicit dynamic analysis. Its advantages will be shown in the following examples.

4. Free vibration analysis

If no damping or forcing terms exists in Eq. (8), after introducing the smoothed versions of strain and stress, it reduces to

$$\mathbf{M}\ddot{\mathbf{d}} + \tilde{\mathbf{K}}\mathbf{d} = \mathbf{0}, \tag{21}$$

where the smoothed stiffness matrix is given as

$$\tilde{\mathbf{K}}_{IJ} = \sum_{C} \int_{\Omega_C} \tilde{\mathbf{B}}_I^{\mathrm{T}} \mathbf{D} \tilde{\mathbf{B}}_J \, \mathrm{d}\Omega, \tag{22}$$

where C is the number of SC that an element is subdivided.

A general solution of such an equation can be written as $\mathbf{d} = \bar{\mathbf{d}} \exp(\mathrm{i}\omega t)$. Then on its substitution into Eq. (21), the frequency ω can be found from

$$(-\omega^2 \mathbf{M} + \tilde{\mathbf{K}})\bar{\mathbf{d}} = \mathbf{0}, \tag{23}$$

where $\bar{\mathbf{d}}$ is the eigenvector.

4.1. Example 1: free vibration analysis of a cantilever beam

In this example, a cantilever beam is studied as shown in Fig. 3, with $L = 100\,\mathrm{mm}$, $H = 10\,\mathrm{mm}$, thickness $t = 1.0\,\mathrm{mm}$, Young's modulus $E = 2.1 \times 10^4\,\mathrm{kgf/mm^4}$, Poisson's ratio $v = 0.3$, mass density $\rho = 8.0 \times 10^{-10}\,\mathrm{kgf\,s^2/mm^4}$. A plane stress problem is considered. Using the Euler–Bernoulli beam theory we can get its fundamental frequency $f_1 = 0.08276 \times 10^4\,\mathrm{Hz}$ as a reference. This problem has also been investigated in Ref. [8]. Several kinds of regular meshes are used in the analysis using both SFEM and FEM. Both 4- and 8-node isoparametric mapped finite elements are employed to examine the accuracy of numerical results and they use 2×2 (Q4) and 3×3 (Q9) Gaussian quadrature for integrating stiffness matrix, respectively [9,10]. A stabilized 4-node quadrilateral element with one-point quadrature was also proposed by Liu and Belytschko to achieve high coarse-mesh accuracy and deal with incompressible materials [11–13]. The stability in space is obtained by using a stabilization matrix that is orthogonal to all linear fields. The frame-invariant QBI element is adopted in this work for comparison purpose.

In FEM, we first investigate the effect of the consistent and lumped mass matrix on the eigenvalues. From the results in Table 1, we notice that their difference is almost negligible. Hence, in following free vibration analysis we always use the consistent mass matrix in FEM. The first four frequencies of the beam are listed in Table 2 and the first eight eigenmodes are demonstrated in Fig. 4. It is observed that SFEM converges much faster than the 4-node Q4 finite elements especially for a very coarse mesh (10×1 elements). For 20×2 and 50×5 elements, SFEM achieves nearly comparable accuracy as the corresponding 8-node Q9 finite elements but the latter needs much more nodes and thus higher computational cost as compared with the 4-node SFEM. The 4-node QBI element gives comparable accuracy as 8-node element for the last three meshes, which is better than both the 4-node Q4 and smoothed elements. The accuracy using very coarse QBI mesh still leaves a lot to be improved. It should be noted that, as the Euler–Bernoulli kinematic assumption is not included either in FEM or in SFEM, a less stiff model is generally produced, which may be responsible for the reason that the numerical results converge to the one that are slightly smaller than the theory solution [14].

In Table 3, 20×5 elements are used for the same analysis with various number SC. It is observed that with the increase of SC, the results gradually approach those of 4-node Q4 finite elements that are based on

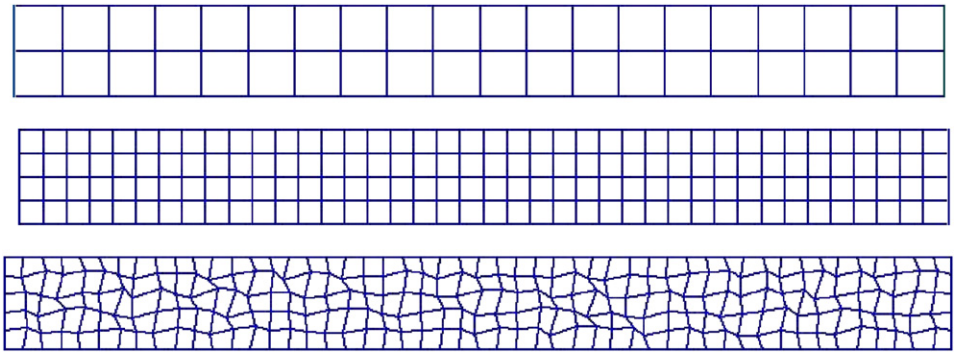

Fig. 3. Meshes of the cantilever beam.

Table 1
First six natural frequencies ($\times 10^4$ Hz) of a cantilever beam using consistent/lumped mass matrix (4-node elements)

No. of elements	No. of nodes	FEM (Q4)		SFEM (4 SC)		Reference (Nagashima [8])
		Lumped mass	Consistent mass	Lumped mass	Consistent mass	
20×2	63	0.0870	0.0872	0.0834	0.0824	0.0926
		0.5199	0.5264	0.4993	0.4990	0.5484
		1.2830	1.2837	1.2828	1.2834	1.2832
		1.3640	1.4011	1.3141	1.3395	1.4201
		2.4685	2.5816	2.3859	2.4697	2.5290
		3.7477	3.8574	3.6333	3.8444	3.7350
50×5	306	0.0830	0.0831	0.0824	0.0823	0.0844
		0.4979	0.4989	0.4944	0.4943	0.5051
		1.2826	1.2827	1.2825	1.2826	1.2828
		1.3111	1.3168	1.3024	1.3054	1.3258
		2.3816	2.3993	2.3670	2.3799	2.3993
		3.6308	3.6701	3.6095	6.6421	3.6432

Table 2
First four natural frequencies ($\times 10^4$ Hz) of a cantilever beam using FEM/SFEM (Euler–Bernoulli beam theory: $f_1 = 0.08276 \times 10^4$ Hz)

No. of elements	No. of nodes	SFEM (4 SC)	FEM (4-node Q4)	FEM (8-node Q9)	FEM (4-node QBI)
10×1	22 (4-node ele.)	0.0861	0.1000	0.0827	0.0817
	53 (8-nodes ele.)	0.5071	0.6077	0.4982	0.4824
		1.2828	1.2863	1.2832	1.2526
		1.3124	1.6423	1.3205	1.2826
20×2	63 (4-node ele.)	0.0834	0.0872	0.0823	0.0822
	165 (8-nodes ele.)	0.4993	0.5264	0.4940	0.4928
		1.2828	1.2837	1.2827	1.2827
		1.3141	1.4011	1.3020	1.2982
50×5	306 (4-node ele.)	0.0824	0.0831	0.0822	0.0822
	861 (8-node ele.)	0.4944	0.4989	0.4934	0.4934
		1.2825	1.2827	1.2825	1.2825
		1.3024	1.3168	1.2997	1.2998
100×10	1111 (4-node ele.)	0.0823	0.0824	—	0.8222
		0.4935	0.4947		0.4933
		1.2824	1.2825		1.2824
		1.3000	1.3037		1.2993

displacement-compatible model, though the latter may not be necessarily more accurate as compared with the analytical solutions. Such a phenomenon is also observed in the static analysis of 2D beams. We also notice that 4-node Q1 FEM and 1-SC SFEM give exactly the same results. We have proved that as SC approaches infinity, the generated stiffness of SFEM will become the same as the 4-node Q4 elements [2].

Irregular mesh is also employed to investigate the accuracy of the two methods. The coordinates of the irregular mesh can be acquired in the following fashion:

$$x' = x + \Delta x r_c \alpha_{ir},$$
$$y' = y + \Delta y r_c \alpha_{ir}, \tag{24}$$

where Δx and Δy are initial regular element sizes in x- and y-direction, respectively. r_c is a computer-generated random number between -1.0 and 1.0 and α_{ir} is a prescribed irregularity factor whose value is chosen between

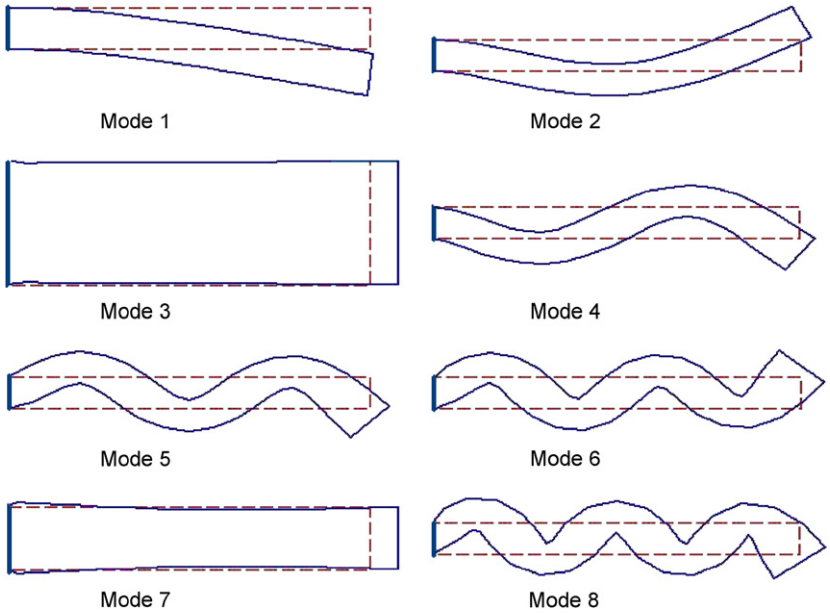

Fig. 4. First eight eigenmodes of the cantilever beam by SFEM.

Table 3
First four natural frequencies ($\times 10^4$ Hz) of a cantilever beam using different number of SC in SFEM (4-node 20×2 elements)

SFEM						FEM (Q4)
SC = 1 (FEM Q1)	SC = 2	SC = 3	SC = 4	SC = 8	SC = 16	
0.0712	0.0746	0.0791	0.0834	0.0841	0.0861	0.0872
0.4294	0.4495	0.4752	0.4993	0.5034	0.5148	0.5264
1.1401	1.1911	1.2549	1.2828	1.2829	1.2829	1.2837
1.2819	1.2825	1.2826	1.3141	1.3242	1.3518	1.4011

Table 4
First four natural frequencies ($\times 10^4$ Hz) of a cantilever beam using irregular nodal distribution (50×5 elements)

	$\alpha = 0$	$\alpha = 0.1$	$\alpha = 0.2$	$\alpha = 0.3$	$\alpha = 0.4$
SFEM (4 SC)	0.0824	0.0825	0.0829	0.0829	0.0835
	0.4944	0.4947	0.4955	0.4966	0.4988
	1.2825	1.2825	1.2825	1.2825	1.2825
	1.3024	1.3031	1.3051	1.3082	1.3124
FEM (4-node Q4)	0.0831	0.0831	0.0833	0.0836	0.0839
	0.4989	0.4992	0.5002	0.5016	0.5041
	1.2827	1.2827	1.2827	1.2827	1.2827
	1.3168	1.3176	1.3202	1.3243	1.3295
FEM (4-node QBI)	0.0822	0.0823	0.0824	0.0827	0.0829
	0.4934	0.4936	0.4944	0.4954	0.4976
	1.2825	1.2825	1.2825	1.2825	1.2825
	1.2998	1.3004	1.3024	1.3051	1.3095

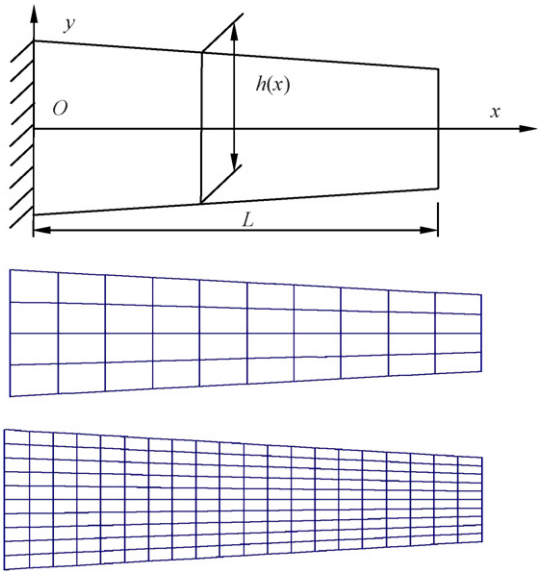

Fig. 5. A cantilever beam with variable cross-section and its meshes.

Table 5
First four natural frequencies ($\times 10^3$ rad/s) of a variable cross-section cantilever beam using FEM/SFEM

No. of elements	No. of nodes	SFEM (4 SC)	FEM (4-node Q4)	FEM (8-node Q9)	FEM (4-node QBI)
10×4	55 (4-node ele.)	0.2611	0.2651	0.2618	0.2607
	149 (8-nodes ele.)	0.9156	0.9489	0.9188	0.9136
		0.9513	0.9540	0.9522	0.9511
		1.8296	1.9576	1.8557	1.8241
20×10	231 (4-node ele.)	0.2617	0.2625	0.2616	0.2615
	661 (8-nodes ele.)	0.9176	0.9249	0.9178	0.9167
		0.9518	0.9525	0.9520	0.9518
		1.8477	1.8774	1.8526	1.8455
40×20	861 (4-node ele.)	0.2616	0.2618	—	0.2616
		0.9177	0.9195		0.9175
		0.9519	0.9521		0.9519
		1.8512	1.8587		1.8506

0.0 and 0.5. The bigger the value of α_{ir}, the more irregular the shape of generated elements. Table 4 gives the results using 50×5 elements. It is seen that with the increase of α_{ir}, the accuracy reduces for both methods whereas SFEM always gives better results than Q4 FEM. The 4-node QBI solutions are comparably closer to SFEM than to 4-node Q4 elements.

4.2. Example 2: free vibration analysis of a variable cross-section beam

A cantilever beam with variable cross-section is examined as shown in Fig. 5. The following parameters are used: $L = 10$; $H(0) = 5$, $H(L) = 3$, $t = 1.0$, $E = 3.0 \times 10^7$, $v = 0.3$, and $\rho = 1.0$. The first four natural frequencies are computed using 4-node Q4 finite elements and SFEM as given in Table 5. Similar to the first example, SFEM gives better results than 4-node Q4 elements when using the same mesh and they are comparable with the 4-node QBI and 8-node finite elements.

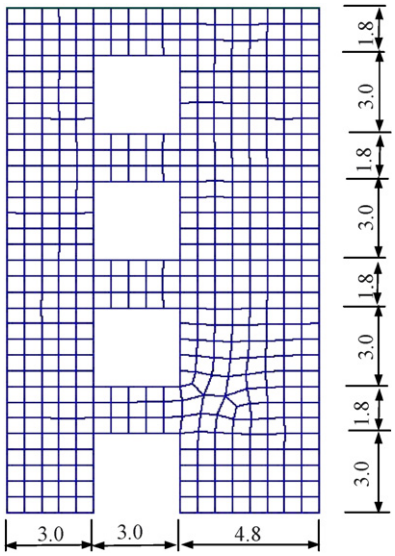

Fig. 6. A shear wall with four openings.

Table 6
First six natural frequencies ($\times 10^4$ rad/s) of a shear wall using FEM/SFEM

No. of elements	No. of nodes	SFEM (4 SC)	FEM (4-node Q4)	Reference (Brebbia et al. [15])
309 (Mesh 1)	248	2.0877	2.1103	2.079
		7.1175	7.2127	7.181
		7.6300	7.6427	7.644
		12.0501	12.2981	11.833
		15.3932	15.7662	15.947
		18.4207	18.6994	18.644
474 (Mesh 2)	557	2.0597	2.0744	—
		7.0598	7.1153	
		7.6197	7.6270	
		11.8278	11.9766	
		15.2376	15.4448	
		18.2748	18.4285	

4.3. Example 3: free vibration analysis of a shear wall

In this example, a shear wall with four openings (see Fig. 6) is analyzed, which has been solved using BEM by Brebbia et al. [15]. The bottom edge is fully clamped. Plane stress case is considered with $E = 10{,}000$, $v = 0.2$, $t = 1.0$, and $\rho = 1.0$. The first six natural frequencies are listed in Table 6. It is found that the present solutions are in good agreement with those obtained by BEM. From the relationship between accuracy and node number, once again we can conclude that SFEM produces better results than 4-node Q4 FEM.

4.4. Example 4: free vibration analysis of a connecting rod

A free vibration analysis of a connecting rod is performed as shown in Fig. 7. Plane stress problem is considered with $E = 10\,\text{GPa}$, $v = 0.3$, $\rho = 7.8 \times 10^3\,\text{kg/m}^3$. The nodes on the left inner circumference are fixed in two directions. From the results in Table 7, it is observed that SFEM gives comparable results as compared with 4-node Q4 finite elements.

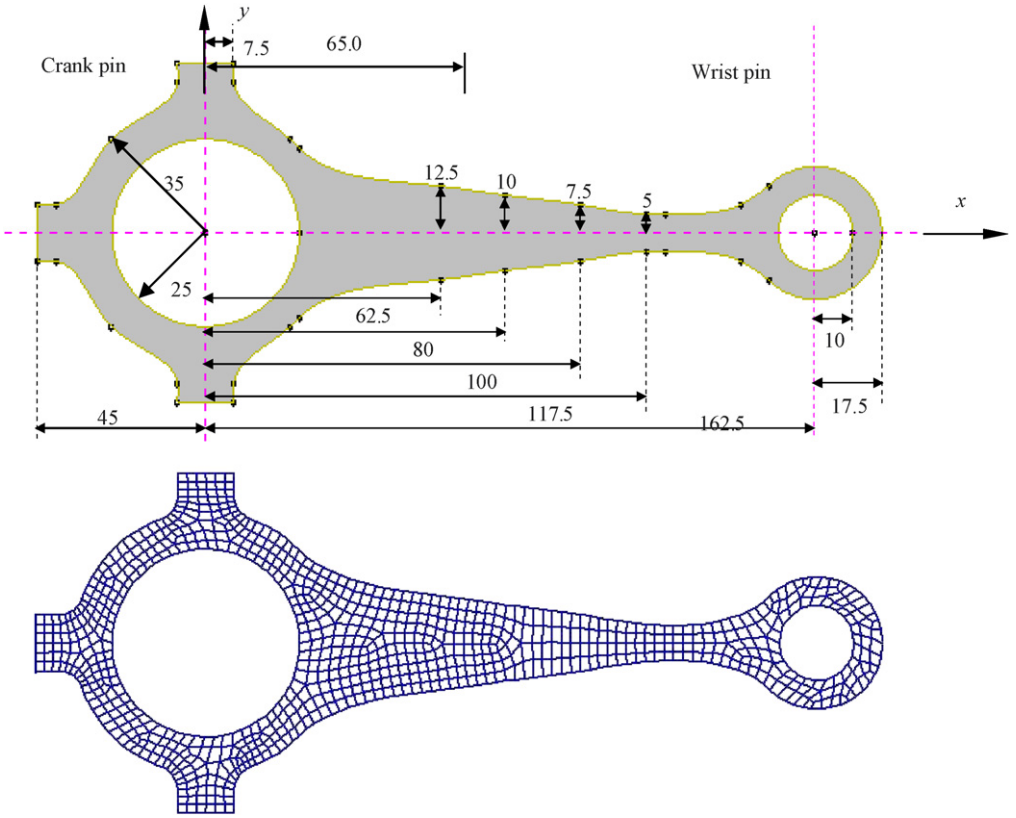

Fig. 7. A connecting rod and its meshes.

Table 7
First six natural frequencies ($\times 10^6$ rad/s) of a connecting rod using FEM/SFEM

No. of elements	No. of nodes	SFEM (4 SC)	FEM (4-node Q4)
353 (Mesh 1)	454	0.1573	0.1596
		0.7047	0.7186
		1.7269	1.7253
		1.7484	1.7751
		3.1807	3.2473
803 (Mesh 2)	970	0.1564	0.1563
		0.7007	0.7050
		1.7230	1.7218
		1.7275	1.7413
		3.1401	3.1733

5. Implicit forced vibration analysis

With the employment of Eqs. (8) and (19), the linear elastic discrete equation in SFEM can be expressed as

$$\mathbf{M}\ddot{\mathbf{d}} + \mathbf{C}\dot{\mathbf{d}} + \tilde{\mathbf{K}}\mathbf{d} = \mathbf{f}^{\text{ext}}. \tag{25}$$

For simplicity a constant damping matrix $\mathbf{C}$ is used that is assumed to be a linear combination of $\mathbf{M}$ and $\tilde{\mathbf{K}}$,

$$\mathbf{C} = \alpha\mathbf{M} + \beta\tilde{\mathbf{K}}, \tag{26}$$

where α and β are the Rayleigh damping coefficients.

Many methods can be used to advance the second-order time-dependent problems with respect to time, such as Newmark method, Crank–Nicholson method, etc. [16]. In this work, Wilson method is used as briefly discussed below [17]. When the state at $t = t_0$ $(\mathbf{d}_0, \dot{\mathbf{d}}_0, \ddot{\mathbf{d}}_0)$ is known, we aim to find the new state $t_1 = t_0 + \Delta t$ $(\mathbf{d}_1, \dot{\mathbf{d}}_1, \ddot{\mathbf{d}}_1)$ by first linearly extrapolating to a hypothetical state $t_2 = t_0 + \theta\Delta t$ $(\mathbf{d}_2, \dot{\mathbf{d}}_2, \ddot{\mathbf{d}}_2)$, where $1.4 \leqslant \theta \leqslant 2$. The following formulations are necessary:

$$\begin{aligned}\left[\left(\frac{6}{\theta^2\Delta t^2}+\frac{3\alpha}{\theta\Delta t}\right)\mathbf{M}+\left(\frac{3\beta}{\theta\Delta t}+1\right)\mathbf{K}\right]\mathbf{d}_2 &= \mathbf{f}_0+\theta(\mathbf{f}_1-\mathbf{f}_0)\\ &+\mathbf{M}\left[\left(\frac{6}{\theta^2\Delta t^2}+\frac{3\alpha}{\theta\Delta t}\right)\mathbf{d}_0+\left(\frac{6}{\theta\Delta t}+2\alpha\right)\dot{\mathbf{d}}_0+\left(2+\frac{\alpha\theta\Delta t}{2}\right)\ddot{\mathbf{d}}_0\right]\\ &+\mathbf{K}\left[\frac{3\beta}{\theta\Delta t}\mathbf{d}_0+2\beta\dot{\mathbf{d}}_0+\frac{\beta\theta\Delta t}{2}\ddot{\mathbf{d}}_0\right],\end{aligned} \tag{27}$$

$$\ddot{\mathbf{d}}_2 = \frac{6}{\theta^2\Delta t^2}(\mathbf{d}_2-\mathbf{d}_0)-\frac{6}{\theta\Delta t}\dot{\mathbf{d}}_0-2\ddot{\mathbf{d}}_0, \tag{28}$$

$$\ddot{\mathbf{d}}_1 = \ddot{\mathbf{d}}_0+\frac{1}{\theta}(\ddot{\mathbf{d}}_2-\ddot{\mathbf{d}}_0), \tag{29}$$

$$\dot{\mathbf{d}}_1 = \dot{\mathbf{d}}_0+\frac{\Delta t}{2}(\ddot{\mathbf{d}}_1+\ddot{\mathbf{d}}_0), \tag{30}$$

$$\mathbf{d}_1 = \mathbf{d}_0+\Delta t\dot{\mathbf{d}}_0+\frac{\Delta t^2}{3}\ddot{\mathbf{d}}_0+\frac{\Delta t^2}{6}\ddot{\mathbf{d}}_1. \tag{31}$$

5.1. Example 5: implicit forced vibration analysis of a cantilever beam

A benchmark cantilever beam is investigated using the Wilson method. It is subjected to a tip harmonic loading $f(t) = \cos\omega_f t$ in y-direction. Plane strain problem is considered with numerical parameters as $L = 4.0$, $H = 1.0$, $t = 1.0$, $E = 1.0$, $v = 0.3$, $\rho = 1.0$, $\alpha = 0.005$, $\beta = 0.272$, $\omega_f = 0.05$, $\theta = 1.4$. The domain is represented with 10×2 elements. In FEM both 4-node Q4 and 8-node Q9 elements are used for comparison. The time step $\Delta t = 1.57$ is used for time integration. From the dynamic responses in Fig. 8 it is seen that both

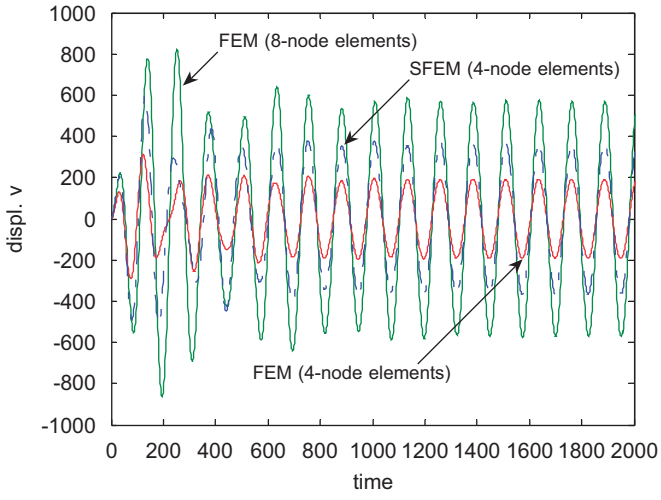

Fig. 8. Comparison of transient responses of a cantilever beam by 4-node Q4 FEM/SFEM.

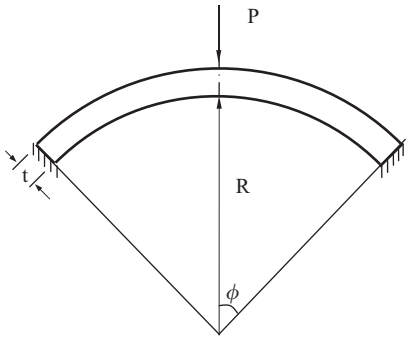

Fig. 9. A spherical shell.

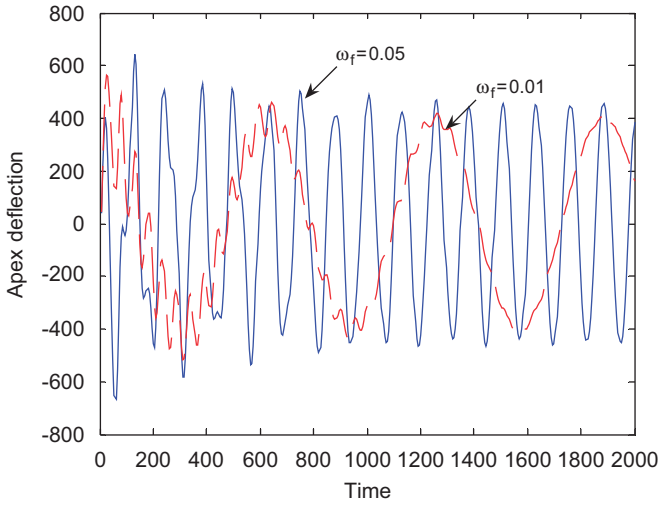

Fig. 10. Transient responses of the spherical shell subjected to a harmonic loading.

methods give nearly identical vibration frequency but the amplitude of SFEM seems closer to that of the 8-node finite elements as compared to the 4-node finite elements.

5.2. *Example 6: implicit forced vibration analysis of a spherical shell*

As shown in Fig. 9, a spherical shell is studied that subjected to a concentrated loading at its apex. In total, 30×3 asymmetric elements are used with numerical parameters given as $R = 12$, $t = 0.1$, $\phi = 10.9^\circ$, $\theta = 1.4$, $E = 1.0$, $v = 0.3$, $\rho = 1.0$. The loading is first in the harmonic form $f(t) = \cos \omega_f t$ and its dynamic responses are demonstrated in Fig. 10 with $\omega_f = 0.01$ and 0.05, respectively, and time step $\Delta t = 5$. No damping effect is included. Then a constant step load $f(t) = 1$ is added at apex since $t = 0$. It is seen from Fig. 11 that with the elapse of time the deflection at apex tends to be a constant value. With the inclusion of damping ($\alpha = 0.005$, $\beta = 0.272$), the response is damped out more quickly.

6. Explicit nonlinear forced vibration analysis

Total Lagrange formulation is used when geometrical nonlinear behavior is considered. The initial position of a material point in a body is given by $\mathbf{X}$ in a fixed reference configuration and the total displacement at time

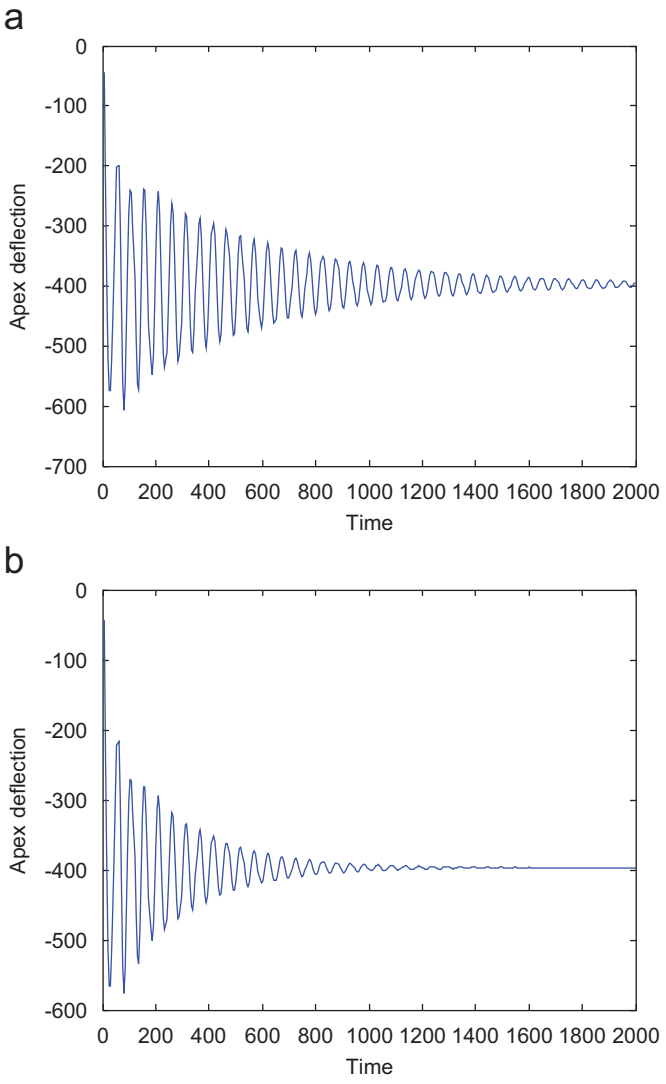

Fig. 11. Transient responses of the spherical shell subjected to a constant step loading: (a) without damping; (b) with damping.

t_n is denoted as $\mathbf{u}_n$ then the current deformed configuration is described by

$$\mathbf{x}_n = \mathbf{X} + \mathbf{u}_n. \tag{32}$$

The current deformation is measured by the deformation gradient matrix relative to $\mathbf{X}$ given by

$$\mathbf{F}_n = \frac{\partial \mathbf{x}_n}{\partial \mathbf{X}}. \tag{33}$$

In the reference configuration the Green strain may be expressed as

$$\mathbf{E}_n = \frac{1}{2}(\mathbf{F}_n^{\mathrm{T}}\mathbf{F}_n - \mathbf{I}). \tag{34}$$

Accordingly the strain–displacement matrix consists of two parts, the linear and nonlinear parts:

$$\mathbf{B} = \mathbf{B}_L + \mathbf{B}_{NL}, \tag{35}$$

whose Ith component is given below for 2D problems

$$\mathbf{B}_I(\mathbf{d}_n) = \begin{bmatrix} F_{11}\dfrac{\partial N_I}{\partial X_1} & F_{21}\dfrac{\partial N_I}{\partial X_1} \\ F_{12}\dfrac{\partial N_I}{\partial X_2} & F_{22}\dfrac{\partial N_I}{\partial X_2} \\ F_{12}\dfrac{\partial N_I}{\partial X_1} + F_{11}\dfrac{\partial N_I}{\partial X_2} & F_{22}\dfrac{\partial N_I}{\partial X_1} + F_{21}\dfrac{\partial N_I}{\partial X_2} \end{bmatrix}. \tag{36}$$

In a similar way, deformation gradient in Eq. (36) needs to be smoothed in SFEM as

$$\begin{aligned} \tilde{F}_{ij}(\mathbf{X}_C) &= \frac{1}{A_C^X}\int_{\Omega_C^X}\left[\frac{\partial u_i^h}{\partial X_j} + \delta_{ij}\right]\mathrm{d}\Omega = \frac{1}{A_C^X}\int_{\Omega_C^X}\left[\frac{\partial u_i^h}{\partial X_j}\right]\mathrm{d}\Omega + \delta_{ij} \\ &= \frac{1}{A_C^X}\int_{\Gamma_C^X}(u_i^h n_j)\,\mathrm{d}\Gamma + \delta_{ij} = \tilde{e}_{ij}(\mathbf{X}_C) + \delta_{ij}, \end{aligned} \tag{37}$$

where $A_C^X = \int_{\Omega_L^X}\mathrm{d}\Omega$ is the initial area of the smoothing cell in study and

$$\tilde{e}_{ij}(\mathbf{X}_C) = \frac{1}{A_C^X}\int_{\Gamma_C^X}(u_i^h n_j)\,\mathrm{d}\Gamma \quad \text{or} \quad \tilde{e}_{ij}(\mathbf{X}_C) = \sum_I \tilde{b}_{jI}^C d_{iI}, \tag{38}$$

where $\tilde{b}_{jI}^C = 1/A_C^X\int_{\Gamma_C^X}(N_I n_j)\,\mathrm{d}\Gamma$. Note that the outward unit normal n_j is defined in initial configuration.

Once the Green strain $\tilde{\mathbf{E}}_n$ is obtained using the smoothed deformation gradient in Eq. (34), the Piola–Kirchhoff stresses can be accordingly computed using $\tilde{\boldsymbol{\sigma}}_n = \mathbf{D}\tilde{\boldsymbol{\varepsilon}}_n$.

6.1. Example 7: explicit forced vibration analysis of a spherical shell

To clearly demonstrate the effect of geometrical nonlinearity as compared with the linear elastic analysis, we change the material properties as well as the geometric parameters of the spherical shell in this example as follows: $R = 12.1\,\mathrm{cm}$ in, $t = 0.04\,\mathrm{cm}$, $\phi = 10.9^\circ$, $P = 445\,\mathrm{N}$, $E = 68.9\,\mathrm{GPa}$, $v = 0.3$. $\rho = 2.82\times10^3\,\mathrm{kg/m^3}$. A

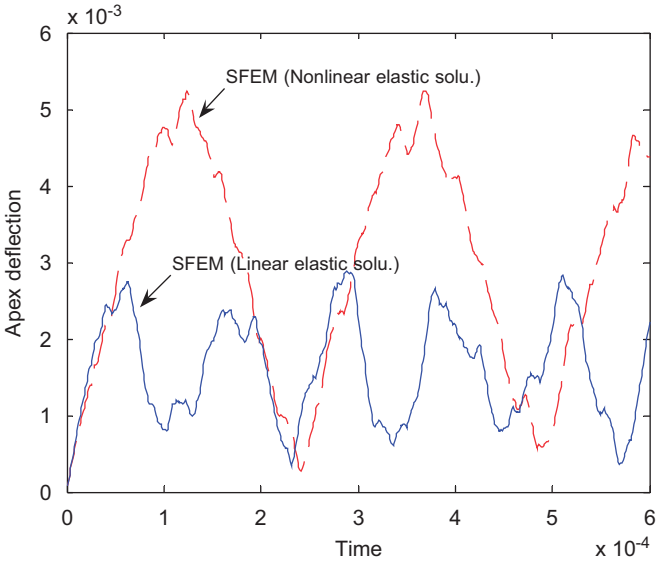

Fig. 12. Linear and nonlinear elastic dynamic responses of a spherical shell under concentrated loading.

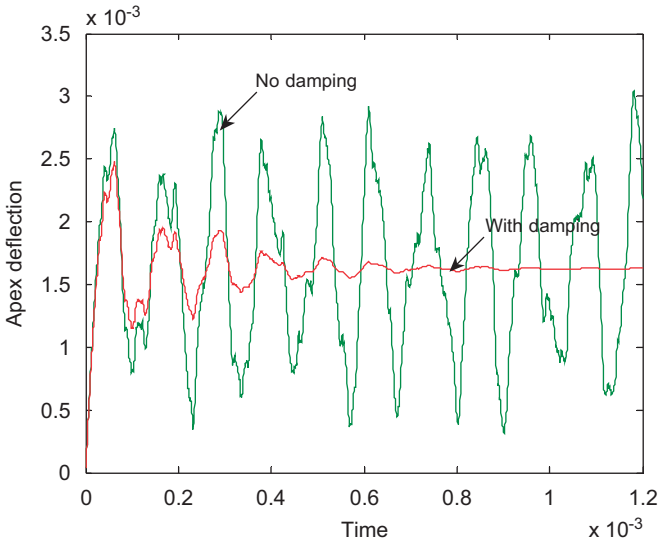

Fig. 13. Linear elastic dynamic responses of a spherical shell with damping.

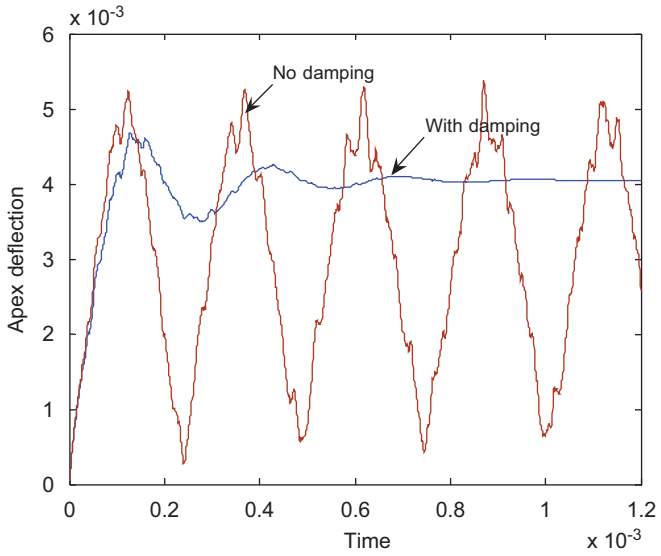

Fig. 14. Nonlinear elastic dynamic responses of a spherical shell with damping.

central difference procedure is used to integrate the kinematics explicitly through time. As the method is conditionally stable a very small time step is permitted that solely depends on the computational model. In this example, $\Delta t = 10^{-8}$ s is used. Fig. 12 shows the comparison of dynamic responses between linear and nonlinear elastic solutions. It is observed that both the period and amplitude of nonlinear response are about two times of those of linear case. In Figs. 13 and 14, dynamic relaxation is introduced with $\alpha = 10^4$ and $\beta = 0$. We notice that the response is damping out gradually and static deflection can be approximately retrieved. The static linear deflection is located roughly at the middle part of the curves whereas the static nonlinear deflection is very close to the peak amplitude, which is agreeable with those using static nonlinear analysis of Newton–Raphson procedure [18]. When the loading is relatively very large, the apex of the shell deforms from the upper side to the lower (see Fig. 15) and the linear analysis cannot yield a reasonable solution.

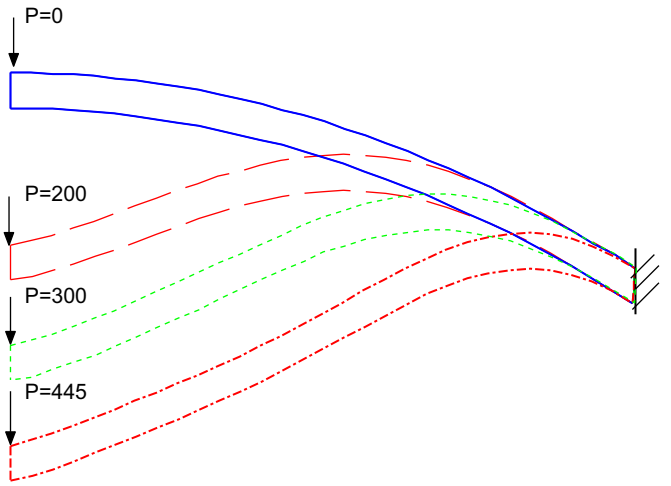

Fig. 15. The deformed shell geometries.

7. Conclusions

The newly developed SFEM is further applied to the free and forced vibration analysis of 2D problems in this work. Compared with the conventional finite elements, the following remarks can be made:

(1) In the natural frequency analysis it is found that SFEM gives much more accurate results and higher convergence rate than the corresponding 4-node Q4 finite elements. For some cases, comparable accuracy of SFEM can be acquired as compared with that of 8-node Q9 finite element but the former uses much smaller number of nodes and thus more computationally efficient.
(2) In the forced vibration analysis, vibration period using SFEM is in good accord as compared with that of 4-node Q4 finite elements but the former vibration amplitude is closer to the responses of the 8-node Q9 elements.
(3) Deformation gradient is smoothed on the level of SC as performed for strain. Explicit geometrical nonlinearity is also well incorporated in dynamic analysis. Nonlinear static deformation can be achieved by introducing dynamic relaxation.
(4) By comparison the numerical procedure of SFEM is very easy and straightforward to implement. Field gradients are computed directly using the shape function itself, rather than its derivatives, which are created in a very simple and explicit manner. All these modifications would not incur addition computational cost. So far we did not encounter any restrictions on this method in dynamic problems.

References

[1] G.R. Liu, K.Y. Dai, T.T. Nguyen, A smoothed finite element method for mechanics problems, *Computational Mechanics* (2006) (in press).
[2] G.R. Liu, T.T. Nguyen, K.Y. Dai, K.Y. Lam, Theoretical aspects of the smoothed finite element method (SFEM), *International Journal for Numerical Methods in Engineering* (2006) (accepted for publication).
[3] J.S. Chen, C.T. Wu, S. Yoon, Y. You, A stabilized conforming nodal integration for Galerkin meshfree method, *International Journal for Numerical Methods in Engineering* 50 (2001) 435–466.
[4] J. Bonet, R.D. Wood, *Nonlinear Continuum Mechanics for Finite Element Analysis*, Cambridge University Press, Cambridge, 1997.
[5] Y. Li, G.R. Liu, K.Y. Dai, M.T. Luan, Z.H. Zhong, G.Y. Li, X. Han, Contact analysis for solids based on linearly conforming RPIM, *Computational Mechanics* (2006) (in press).
[6] G.R. Liu, G.Y. Zhang, K.Y. Dai, Y.Y. Wang, Z.H. Zhong, G.Y. Li, X. Han, A linearly conforming point interpolation method (LC-PIM) for 2D solid mechanics problems, *International Journal of Computational Methods* 2 (2006) 645–665.

[7] K.Y. Dai, G.R. Liu, Z.H. Zhong, G.Y. Li, X. Han, An *n*-sided polygonal smoothed finite element method (nSFEM) for solid mechanics, *Finite Elements in Analysis and Design* (2006) (submitted for publication).
[8] T. Nagashima, Node-by-node meshless approach and its application to structural analysis, *International Journal for Numerical Methods in Engineering* 46 (1999) 341–385.
[9] O.C. Zienkiwicz, R.L. Taylor, *The Finite Element Method*, fifth ed., Vol. 1, Butterworth Heinemann, Oxford, 2000.
[10] K.J. Bathe, *Finite Element Procedures*, Prentice-Hall, Englewood Cliffs, NJ, 1996.
[11] W.K. Liu, T. Belytschko, Efficient linear and nonlinear heat conduction with a quadrilateral element, *International Journal for Numerical Methods in Engineering* 20 (1984) 931–948.
[12] T. Belytschko, W.E. Bachrach, Efficient implementation of quadrilaterals with high coarse-mesh accuracy, *Computer Methods in Applied Mechanics and Engineering* 54 (1986) 279–301.
[13] T. Belytschko, J.S. Ong, W.K. Liu, J.M. Kennedy, Hourglass control in linear and nonlinear problems, *Computer Methods in Applied Mechanics and Engineering* 43 (1984) 251–276.
[14] G.R. Liu, K.Y. Dai, K.M. Lim, Y.T. Gu, A point interpolation mesh free method for static and frequency analysis of two-dimensional piezoelectric structures, *Computational Mechanics* 29 (2002) 510–519.
[15] C.A. Brebbia, J.C. Telles, L.C. Wrobel, *Boundary Element Techniques*, Springer, Berlin, 1984.
[16] T. Belytschko, An overview of semidiscretization and time integration procedures, in: T. Belytschko, T.J.R. Hughes (Eds.), *Computational Methods for Transient Analysis*, Vol. 1, North-Holland, Amsterdam, 1983.
[17] I.M. Smith, D.V. Griffiths, *Programming the Finite Element Method*, third ed., Wiley, New York, 1998.
[18] K. Kleiber, C. Wozniak, *Nonlinear Mechanics of Structures*, Kluwer Academic Publishers, Dordrecht, 1991.